Carbon 215 (2023) 118385

Contents lists available at ScienceDirect

Carbon

journal homepage: www.elsevier.com/locate/carbon

Research paper

Modeling symmetric and defect-free carbon schwarzites into various zeolite templates

Enrico Marazzi [a,*], Ali Ghojavand [a,1], Jérémie Pirard [a], Guido Petretto [a], Jean-Christophe Charlier [a], Gian-Marco Rignanese [a,b]

[a] Institute of Condensed Matter and Nanosciences, UCLouvain, Chemin des Étoiles 8, Louvain-la-Neuve 1348, Belgium
[b] School of Materials Science and Engineering, Northwestern Polytechnical University, No. 127 Youyi West Road, Xi'an 710072 Shaanxi, PR China

ARTICLE INFO

Keywords:
Schwarzites
Zeolite-templated nanostructures
Carbon nanotubes
Random symmetric generation

ABSTRACT

Recently, a process has been proposed for generating negatively-curved carbon schwarzites via zeolite-templating (Braun et al., 2018). However, the proposed process leads to atomistic models which are not very symmetric and often rather defective. In the present work, an improved generation approach is developed, by imposing symmetry constraints, which systematically leads to defect-free, hence more stable, schwarzites. The stability of the newly predicted symmetric schwarzites is also compared to that of other carbon nanostructures (in particular carbon nanotubes — CNTs), which could also be accommodated within the same templates. Our results suggest that only a few of these (such as FAU, SBT and SBS) can fit schwarzites more stable than CNTs. Our predictions could help experimentalists in the crucial choice of the template for the challenging synthesis of schwarzites. Furthermore, being highly symmetric and stable phases, the models could also be synthesized by means of other experimental procedures.

1. Introduction

The discovery of fullerenes, carbon nanotubes and graphene [1–4] sparked an increasing interest in sp^2-like carbon nanostructures due to their peculiar functional and structural properties [5]. The most astonishing example is the linear dispersion of the electronic bands of graphene near the Fermi level that gives rise to outstanding structural (flexibility), electrical, and optical properties. All these nanostructures are only composed of carbon atoms with three nearest-neighbors, but differ by their dimensionality and the Gaussian curvature [6] of the surface generated in the 3D space. Indeed, graphene is 2D with a null Gaussian curvature due to the perfectly planar sp^2 hybridization. Uncapped nanotubes are 1D with a null Gaussian curvature too, but the principal curvature perpendicular to the cylindrical axis is positive as a result of bond angle deviations from 120° (inducing out-of-plane bending). At last, fullerenes are 0D and exhibit a positive Gaussian curvature everywhere, which is the result of the introduction of 12 five-membered rings (pentagons) besides the six-membered rings (hexagons) typically present in flat surfaces. In order to obtain 3D sp^2-like carbon nanostructures, a negative curvature is required (i.e., saddle points). This can be achieved by introducing seven- (heptagons) or eight-membered (octagons) rings beside the hexagonal network. Such 3D negatively-curved sp^2-carbon nanostructures are called schwarzites [7–9].

A few decades ago, theoretical calculations predicted the stability of several schwarzites with respect to other carbon forms (such as C_{60}). They have thus attracted considerable attention due to their appealing predicted electronic [10–12], magnetic [13] and mechanical [14,15] properties, and for their potential applications in batteries [16], gas absorption and storage [17,18] or thermoelectricity [19], just to cite a few. More recently, inspired by the templated carbonization method widely used experimentally to synthesize atomically-controlled nanostructures [20–23], a much wider range of atomistic models were proposed adopting different zeolites as templates [24,25]. Indeed, these SiO_2-based porous crystalline materials exhibit complex crystallographic structures that embed molecule-sized pores [26], which make them suitable to play the key role of templates for the synthesis of potential schwarzites. For instance, Fe-modified FAU and BEA were very recently used for the growth of zeolite-templated carbons from methane decomposition resulting in high-quality compounds with low hydrogen concentration [27]. It is interesting to note that the smallest-radius CNT was also obtained from a zeolite template [28]. In a review

* Corresponding author.
E-mail addresses: enrico.marazzi@uclouvain.be (E. Marazzi), jean-christophe.charlier@uclouvain.be (J.-C. Charlier), gian-marco.rignanese@uclouvain.be (G.-M. Rignanese).
[1] Present address: Department of Physics & NANOlab Center of Excellence, University of Antwerp, Groenenborgerlaan 171, B-2020 Antwerp, Belgium.

https://doi.org/10.1016/j.carbon.2023.118385
Received 20 June 2023; Received in revised form 26 July 2023; Accepted 21 August 2023
Available online 4 September 2023

on zeolite-templated carbon schwarzite models, Taylor et al. [29] argued that the models proposed by Braun et al. [24] do not correspond to zeolite-templated schwarzites obtained so far in experiments, both on the structure (the surface area is smaller than the observed one) and on chemical composition (the models by Braun and collaborators are purely composed of carbon atoms, while the experimental ones have high concentrations in hydrogen and oxygen). In that review, Taylor et al. claimed that these models are important solely as idealized hypothetical schwarzites that may be eventually synthesized. With this in mind, the goal of the present research is to produce models which are more symmetric and hence more stable than those already presented in the literature. That does not necessarily imply that it will be possible to produce the predicted schwarzites starting from the associated zeolite templates. In fact, the templates can also be seen as references for generating new models and, later on, different methodologies might be adopted at the production stage [30–32]. In particular, it has been demonstrated that bottom-up approaches may be viable solutions [31, 32]. Note that, in such a case, a target structure is needed. The stable and highly symmetric schwarzite models proposed in this work could definitely serve this purpose. Another viable solution for synthesizing some of these models might be to perform post-annealing or other thermal treatment starting from zeolite-templated carbon nanostructures such as those obtained by Nishihara and collaborators [20]. Indeed, being synthesized from the right zeolite, such samples would already have the right initial shape and could thus be converted into the models proposed in this work. Finally, the algorithm proposed here can be used to generate schwarzites starting from other porous materials, different from zeolite, and to compute schwarzites based on other elements rather than carbon. For instance, germanium-based schwarzites have attracted interest recently [33]. The zeolites considered as templates in this work originate from the "IZA Database for Zeolite Structures" [34]. Even though the latter includes over 250 structures, only 60 are investigated here, namely, those also selected by Braun et al. [24] via a topological analysis. Those were chosen for the size of their pores and hence the possibility to form 3D nanostructures. Finally, a complete analysis with other possible carbon nanostructures, especially carbon nanotubes (CNTs), is performed. Indeed, carbon nanotubes may also fit into a zeolite template and could have a lower energy than any schwarzitic counterpart. Only after these considerations, it will be possible to state which is the most stable structure for each template.

2. Materials & methods

2.1. Random symmetric-structure generation

The two proposed approaches to produce carbon-based schwarzites rely on random structure generation combined with the systematic use of structural symmetries. Indeed, random search is quite effective when little is known about the system [35,36] and taking into account structural symmetry usually improves the stability of the generated structures [37]. In fact, statistical studies show that more than 2/3 of all inorganic crystal structures can be gathered into 24 space groups (i.e., about 10%) out of the 230 existing ones [38]. The other advantage of working with symmetries is that a small set of symmetrically-inequivalent coordinates are sufficient to describe a structure. This is particularly convenient for our study given that the zeolite templates have large conventional cells and that the resulting schwarzites will typically include hundreds of atoms. The advantage is, however, expected to strongly depend on the degree of symmetry of the structure since only symmetrically-inequivalent positions matter. On the one hand, in systems with lots of symmetry operations, the unit cell is quickly filled by a few atoms. On the other hand, in systems with few symmetry operations, many new atoms are required to fill the unit cell, and therefore many random attempts are needed. Imposing a high degree of symmetry reduces the number of structures that can be explored and, therefore, limits the possibility of obtaining interesting results. However, working in a smaller space makes the search for the most stable structure in the subset much easier. And, if no stable model is found with the space group selected initially, it is always possible to reduce the number of symmetry operations and explore a larger space. Here, the generated schwarzites are first forced to have the same space group as the template but, when needed, this constraint is relaxed considering the compatible subgroups. We computed the zeolite-templated schwarzite models with an in-house developed Python code [39]. To define the space group, a certain tolerance on the atomic positions must be allowed. The space groups that are mentioned in this work are computed considering a tolerance of 0.01 in the unit length. To prevent strong interaction between the template and the schwarzite a 1.6-Å vacuum will be imposed. This choice is based on the crystal ionic radius for oxygen (1.26 Å), silicon (0.54 Å) and carbon (0.3 Å) [40].

The first algorithm adds carbon atoms randomly one by one, but with various geometrical constraints. Firstly, the new atom must be at an appropriate distance from the template and the existing atoms. The symmetry operations belonging to the target space group are then applied and replicas are checked to ensure they are not too close to the template. In case several atoms are too close to one another, their positions are averaged. Lastly, if all the above constraints are fulfilled, the structure is relaxed keeping the symmetry fixed and the algorithm repeats adding a new atom. Otherwise, the structure is discarded, and the algorithm starts from scratch. Improvements to the algorithm involve selecting the position of the added atom based on certain criteria. For instance, it can be placed only close to atoms with less than three nearest neighbors, or it can be placed in a region close to two under-coordinated atoms trying to connect them. The second method employed is a genetic algorithm (GA) which is an optimization algorithm based on the concept of the survival of the fittest. The GA starts with a random population and the best individuals are modified while preserving the desired traits, only the fittest candidates are kept [41–43]. The initial population is a random selection of the best structures generated with the previous algorithm. Subsequently, a structure is chosen and its atoms are modified accordingly to the above-mentioned constraints. Modifications can include moving or removing an atom, merging two atoms, or adding a new atom. Alternatively, the atomic positions of two candidates may be mixed. When selecting the candidates from the population, a fitness function is used to bias toward the most stable structures [44]. After each operation, a relaxation is performed to ensure stability. The space group is carefully preserved and the new candidate is kept only whether its atoms do not get too close to the template. Both algorithms use the AIREBO [45] potential for relaxation. However, in the calculation of the fitness function, the AIREBO potential is replaced with a more reliable potential for carbon, the Gaussian approximation potential (GAP) [46] (more details are provided later in the text). The order in which the two algorithms are used depends on the features of the template, and there is no defined recipe. As a last step, a full DFT relaxation using Vienna Ab Initio Simulation Package (VASP) [47–50] is performed on the best structures for each template. The k-grid is chosen such that it ensured a k-point density of 1000 points/Å in the reciprocal space, a cut-off energy of 600 eV and the computation of van der Waals correction through DFT-D3 method [51] with Becke-Johnson damping. The computations are automatized with atomate2 [52,53] and FireWorks [54]. The choice of a large cut-off is made to prevent numerical instabilities while relaxing the cell volume. The convergence of the self-consistent loop is reached when the difference in energy is smaller than 10^{-7} eV, while for the ionic relaxation loop the tolerance on energy is 0.001 eV. During this relaxation, all the constraints on symmetry and the template are removed. Since the proposed algorithm relies on symmetries, and symmetries are not compatible with defects, it is difficult to compare the generated models with experiments. To better match the experimental conditions, the algorithm could be extended to incorporate defects, or hydrogen and oxygen atoms. A possible solution would be to modify the genetic algorithm to reduce the symmetry and simulate

a defect by removing a C atom or substituting it with H or O atoms. However, this approach would introduce several complications. Firstly, it would require finding a new fitness function that goes beyond energy per atom, and that would be more fit for heterogeneous structures. Moreover, to introduce defects without an excessive density in the crystal, large supercells would be needed to treat the schwarzite models. Since the schwarzite unit cells already contain hundreds of atoms, the computational costs would escalate significantly. Finally, a new potential that is suited to describe the C–H–O interactions would need to be developed. However, this goes beyond the scope of the present work.

2.2. Carbon nanotube accommodation

As mentioned above, the possible formation of carbon nanotubes is also envisaged for each zeolite template. To this end, we first determine whether one given template exhibits channels going through the whole system (beyond the unit cell) and, if so, the radius of the largest channel R_{ch}. Considering that the smallest synthesized CNT has a radius of 2 Å [55,56] (e.g., the tubes with indices (3,3), (5,0) and (4,2)) and adding 1.6 Å of vacuum, we assume that a template can accommodate a CNT when R_{ch} is at least 3.6 Å. Given that the stability of the CNTs increases with their radius, the radius of the CNT that is most likely to form in the template zeolite is taken to be $R_{CNT} = R_{ch} - 1.6$ Å. This CNT can be used as a reference for assessing the thermodynamic stability of the most stable schwarzite model for the considered template. The nanotube energies are calculated by relaxing six CNTs with different radii and then fitting the energy curve with a function of the form $f(r) = a + b/r^2$, where r is the CNT radius and a and b are the fitting parameters (cfr. Fig. B.4 in Appendix B). After determining the largest channel radius for each template, the value of the corresponding energy is extracted from this fit. When it is not possible to accommodate a tube in the template, the buckyball C_{60} is chosen as a reference. If either the CNT or the C_{60} is more stable than the schwarzite model, the latter is very unlikely to form, when kinetic arguments are not taken into account.

2.3. Template geometry

To characterize the geometry of the templates, the largest free sphere diameter (D_f) and the largest included sphere diameter (D_i) have been calculated. These are defined as the maximum diameter of a spherical probe that can diffuse through the template and the diameter of the largest spherical void in the porous material, respectively [57]. These quantities have been calculated using the open-source software Zeo++ [57]. For the computation of D_i and D_f, the atomic radii for both oxygen and silicon have been set to 1.35 Å in order to be consistent with the work by Braun et al. [24] and with the IZA database [34].

2.4. Used potentials

Adaptive Intermolecular Reactive Empirical Bond-Order (AIREBO) [45], a force-field potential for carbon, was used to perform relaxations. This choice of this potential was made because calculating energies at each step with DFT would have been computationally expensive, and AIREBO is one of the most accurate among standard potentials [58]. However, some drawbacks were observed while using this potential. When ordering a set of structures from lowest to highest energy, the AIREBO potential misrepresented the order obtained with a DFT calculation (cfr. Fig. A.3 of Appendix A). Therefore, another potential, a machine-learning potential for carbon constructed using the Gaussian approximation potential (GAP) methodology [46], was adopted. This proved to be more reliable in reproducing the DFT order better than AIREBO (see Fig. A.3 in Appendix A). The GAP potential has been used in the genetic algorithm to evaluate the fitness function and to calculate energies in Fig. A.2 in Appendix A. It is, however, important to mention that AIREBO potential is still about 30 times faster than GAP and therefore it is not feasible to use the latter potential to relax the large amount of structures needed to be generated with this method in order to find the best ones.

3. Results & discussion

In this section, the best-generated models are discussed. The thermodynamic stability of the generated schwarzite models is evaluated by comparison with the buckyball C_{60} and the largest CNT that can be accommodated in the template. We thus compute the energy difference per atom between the schwarzite and C_{60} ($\Delta E'$):

$$\Delta E' = \frac{E(\text{schwarzite})}{N_{at}(\text{schwarzite})} - \frac{E(C_{60})}{N_{at}(C_{60})} \tag{1}$$

and, whenever possible, between the schwarzite and the CNT (ΔE):

$$\Delta E = \frac{E(\text{schwarzite})}{N_{at}(\text{schwarzite})} - \frac{E(\text{CNT})}{N_{at}(\text{CNT})} \tag{2}$$

where E and N_{at} are the energy and the number of atoms of the structures indicated between parentheses.

Any schwarzite model with $\Delta E' < 0$ could potentially be synthesized given that its energy per atom is smaller than the one of C_{60} which has already been synthesized. However, in the zeolite template that can accommodate a CNT, the stability with respect to CNT should also be considered and only those structures with $\Delta E < 0$ are likely to form.

The results for all the models can be found in Table A.1 in Appendix A, and the files containing the atomic coordinates of the generated models are available on the Materials Cloud Archive [59]. Fig. 1 shows the values for the best candidates. In panel (a), ΔE is plotted as a function of the largest channel radius in the template R_{ch}. Given that the amount of vacuum 1.6 Å required to accommodate a CNT in a channel is somewhat debatable, the green area represents the energies of all the CNTs with a radius within $R_{CNT} \pm 0.1$ Å. The difference between the energy per atom, between the C_{60} and the CNT, as a function of the radius:

$$\frac{E(C_{60})}{N_{at}(C_{60})} - \frac{E(\text{CNT})}{N_{at}(\text{CNT})} \tag{3}$$

is depicted with a dashed black line. In panel (b), $\Delta E'$ is plotted for the templates in which a tube cannot be incorporated.

Consistently with the work by Braun et al. [24], the generated structures including disconnected parts or displaying connections formed by one-atom chains (sp-hybridization) or two-dimensional nano-sheets (nanoribbons) are considered to be defective. Five of the structures reported in Fig. 1 fall in this category as well as the majority of the models computed from the studied templates which are not reported in this work. While defective schwarzites and models based on hypothetical templates might also show interesting properties, the primary attention is given to defect-free schwarzites calculated from templates that are confirmed experimentally. On the one hand, for some of the templates which cannot accommodate a CNT (Fig. 1.b) a few schwarzite models which are relatively stable can be generated. As a matter of fact, LTA and RHO are more stable than the C_{60} molecule, making these templates suitable to host stable schwarzites. Nonetheless, they have larger energies if compared to the models where a nanotube can fit (cfr. Table A.1 in Appendix A). In panel (b), only LTA, RHO, and BSV exhibit a space group larger than 200. The method proposed relies on symmetries and higher space group structures are expected to be more stable. However, while this is true for RHO and LTA, it is not the case for BSV due to its geometrical characteristics. It is possible to see how D_f and D_i for BSV are particularly small. As a result, the narrow connections in BSV increase the energy of the structure. This highlights the importance of having a high space group together with a favorable geometry in order to achieve stability. Braun et al. [24] decided to calculate schwarzite models starting from templates that have a minimum

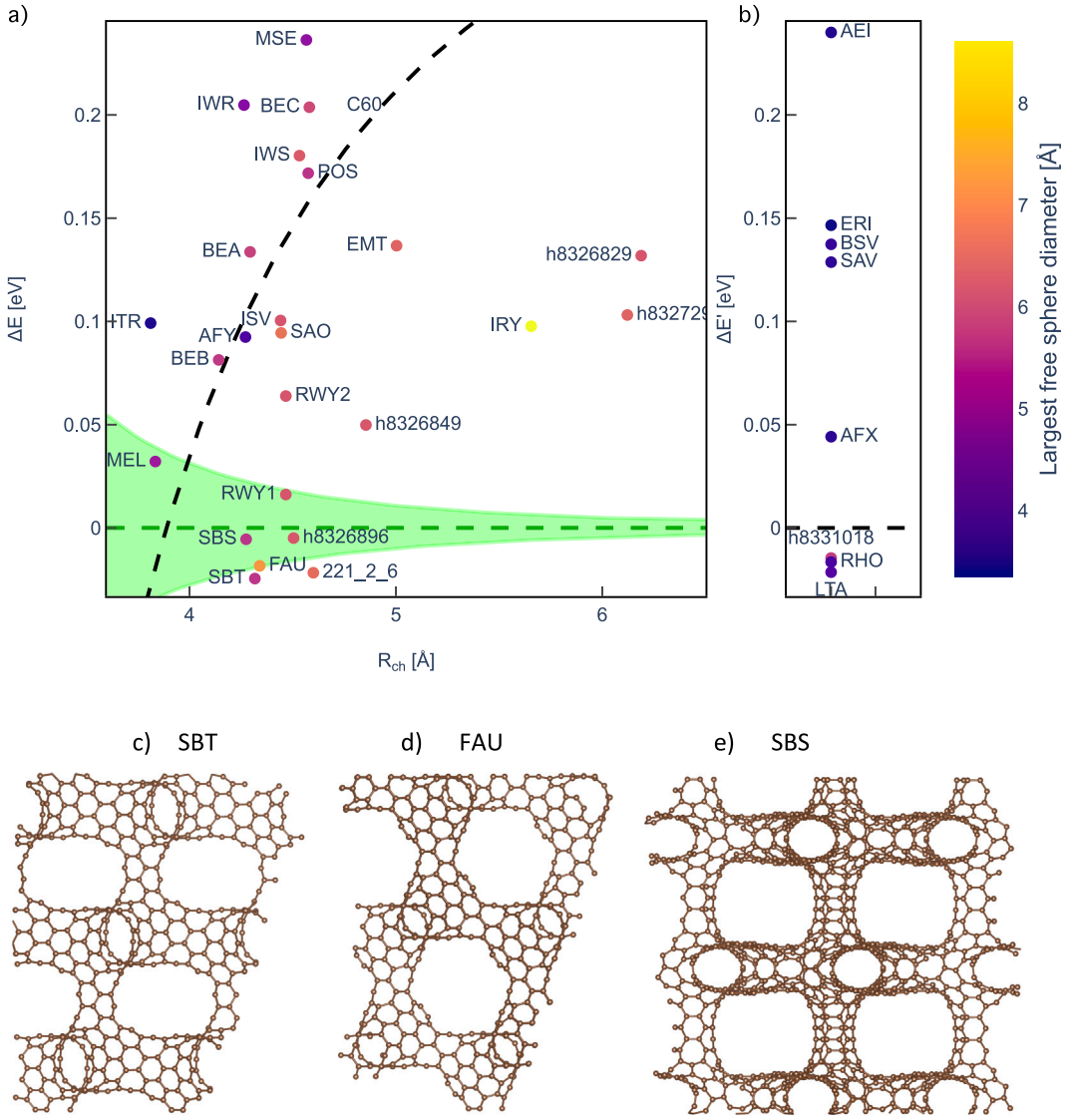

Fig. 1. Best schwarzite candidates: (a) Energy per atom of the different schwarzites for the zeolite templates that can accommodate a CNT. The energy ΔE is reported as a function of R_{ch} (the radius of the largest channel in the zeolite) with respect to the energy of the largest CNT that can be accommodated in the template (i.e., such that the radius of the channel allows for exactly 1.6 Å of vacuum), as defined in Eq. (2). The green area represents the energies per atom of the CNTs with radii that could be up to 0.1 Å smaller or larger. The dashed black line is the energy difference per atom between the C_{60} and the CNTs of varying radius as given by Eq. (3). (b) Energy per atom of the different schwarzites for the zeolite templates that cannot accommodate a CNT. The energy $\Delta E'$ is reported with respect to that of C_{60}, as defined in Eq. (1). In both panels, the color of the circles represents the largest free sphere diameter. All the structures reported in the figure are defect-free schwarzites, except for ERI, ITR, h8326849, h8326896, and h8327291. Panels a and b can be also viewed interactively here [60] through the chemiscope visualization tool [61]. The models for the three schwarzites that are more stable than the CNT and are computed starting from experimentally confirmed zeolites are also shown: (c) SBT, (d) faujasite (FAU) and (e) SBS. (For interpretation of the references to color in this figure legend, the reader is referred to the web version of this article.)

D_f of 5.0 Å, thus limiting the number of possible schwarzite candidates. On the contrary, stable and defect-free schwarzites are investigated in this work regardless of the D_f, allowing for the prediction of stable models for narrower templates as well.

On the other hand, only a few structures are more stable than CNT, if one can be accommodated (cfr. Fig. 1a). Specifically, SBT, FAU, SBS (cfr. Fig. 1.c,d,e), h8326896, and 221_2_6 have a lower energy. Although the latter two structures originate from hypothetical zeolites and may be less interesting, SBT and SBS offer new models for schwarzites. Moreover, while it was already known that Faujasite could potentially host a stable schwarzite, the model computed in this study is more symmetric (with a higher space group) and thus is more stable than those previously reported in the literature. Regarding the other templates, the most stable structure will be a tube, if it can be placed in the zeolite. Moreover, for $R_{ch} > 4.6$ Å, the CNT energy is significantly smaller than the best schwarzite. Therefore, schwarzites can only compete with nanotubes when the tube diameter is not too large.

In Fig. 1, the largest free sphere diameter (D_f) is represented with a colormap. The templates with the largest D_f, the lighter ones, as already studied by Braun et al. [24], generally accommodate schwarzites with the lowest energies. This is because carbon atoms have more

Table 1
Energy per atom, radius of the largest CNT, largest free sphere diameter (D_f) and space group of the best schwarzites model.

Name	Energy per atom [eV]	Radius CNT [Å]	D_f [Å]	Space group
SBT	−9.075	2.72	5.65	166 ($R\bar{3}m$)
FAU	−9.073	2.74	7.29	227 ($Fd\bar{3}m$)
SBS	−9.047	2.67	5.65	163 ($P\bar{3}1c$)
IRY	−9.104	4.06	8.61	194 ($P6_3/mmc$)
RWY1	−9.062	2.87	6.23	221 ($Pm\bar{3}m$)

space to be accommodated and the connections in the necks of the zeolites can be formed by larger tubes, which are more stable (cfr. Fig. A.1 in Appendix A). Moreover, this work increases the number of templates that can host a defect-free schwarzite with respect to literature works (bringing it to 30). As a matter of fact, all structures presented in Figs. 1.a,b are defect-free, with the only exception of ERI, ITR, h8326849, h8326896 and h8327291. These structures are mentioned because of their interesting energy: h8326896 is even more stable than the CNT. By examining the models presented in Fig. 1.c,d,e and Table 1, it can be noted that the most stable structures possess high symmetry and are free from defects. As already mentioned, our method is efficient for systems with a high space group. In Fig. A.2 in Appendix A, the difference in energy per atom between the models from the work of Braun et al. [24], Wu et al. [25] and this one is plotted as a function of the space group number, while the difference in energy per atom between the structure from the literature and the diamond are plotted as a colormap. Note that, here, the energies are calculated with the GAP potential [46]. Focusing only on the defect-free and highly-symmetric models computed in this work, the stability of our structures is improved by ~0.12 eV/atom compared to previous works [24,25]. On the one hand, it can be observed that the proposed method improves the models present in literature if it is able to find a defect-free structure, especially those with high symmetry (the most bettered structure -BSV- is also the one with the largest space group). On the other hand, the procedure is particularly ineffective for templates with a very low space group. It is worth noting that the models that could not be improved in this research have relatively high energy per atom to begin with. This suggests that the difficulty in finding a stable model may come from constraints of the templates, rather than from a fault in the method.

4. Conclusion

This work focuses on the computation of symmetrical and defect-free schwarzite models using zeolites as a starting template. Carbon atoms are gradually added to the unit cell while fulfilling various geometrical constraints. Once an atom is added, the symmetry operations from the target space group are applied and the model is relaxed. This process is repeated for each subsequent atom. Additionally, a genetic algorithm is used to modify the structures of the best models selected from the above process, which further enhances the stability of the candidates. Moreover, the study involves analyzing the geometry of the templates to determine if they can accommodate a carbon nanotube. If a CNT can fit in the template, the energies of the most stable schwarzite and nanotube are compared to identify the best-fitting nanocarbon. This step is particularly significant, as in most cases, the CNT is found to be the most stable nanostructure. Including symmetries in the computation of schwarzites is crucial for enhancing the stability of the models and identifying a broader range of suitable templates. For this reason, the method has proven to be successful for structures with a high space group and vice versa. However, upon examining all the templates presented in Fig. 1.a and b, it becomes evident that for the majority of them, the CNT remains the most stable structure. It is thus important to include the other carbon nanostructures in the calculations to determine the most stable carbon allotrope. The fact that nanotubes are more energetically favorable than schwarzites for a large portion of templates represents a significant challenge to synthesizing these new materials. Nonetheless, there are three models, namely SBS, SBT, and FAU, that are more stable than the nanotube and are generated starting from experimentally-confirmed zeolites. These models are the most promising candidates for further research, with SBS and SBT being newly proposed models in this study. Last but not least, from a theoretical point of view, our work has considerably enlarged the number of known symmetric schwarzites. Indeed, we have proposed 30 new highly-symmetric structures to add to the two (D and P models) theorized previously [7–9].

CRediT authorship contribution statement

Enrico Marazzi: Software, Validation, Investigation, Writing – original draft, Visualization. **Ali Ghojavand:** Investigation, Writing – review & editing. **Jérémie Pirard:** Software, Investigation, Writing – review & editing. **Guido Petretto:** Methodology, Software, Validation, Investigation, Writing – review & editing. **Jean-Christophe Charlier:** Conceptualization, Methodology, Writing – review & editing, Supervision, Project administration, Funding acquisition. **Gian-Marco Rignanese:** Conceptualization, Methodology, Writing – review & editing, Supervision, Project administration, Funding acquisition.

Declaration of competing interest

The authors declare that they have no known competing financial interests or personal relationships that could have appeared to influence the work reported in this paper.

Acknowledgments

The authors acknowledge fundings from the European Union's Horizon 2020 Research Project and Innovation Program — Graphene Flagship Core3 (N° 881603), from the Flag-Era JTC projects "TATTOOS" (N° R.8010.19) and "MINERVA" (N° R.8006.21), from the Fédération Wallonie-Bruxelles through the ARC project "DREAMS" (N° 21/26-116) and the EOS project "CONNECT" (N° 40007563), and from the Belgium F.R.S.-FNRS through the research project "Moiré" (N° T.029.22F). Computational resources have been provided by the CISM supercomputing facilities of UCLouvain and the CÉCI consortium funded by F.R.S.-FNRS of Belgium (N° 2.5020.11)

Appendix A

See Figs. A.1–A.3 and Table A.1

Appendix B. Carbon nanotube fitting energy

The energies for the carbon nanotubes have been calculated by relaxing six nanotubes, the (3,3), (4,4), (5,5), (6,6), (7,7) and (8,8) and then interpolating their energy per atom with the function

$$E(r;a,b) = a + \frac{b}{r^2} \tag{4}$$

where r is the CNT radius while a and b are the fitting parameters. The six tubes have been chosen because of their different radii. The relaxations have been performed with VASP, using the same parameters as those introduced in the main text for the relaxation of schwarzites. In Fig. B.4, the explicitly calculated points are shown as well as the fitting line. The obtained parameters for a and b are −9.325 eV and 2.026 eV · Å^2, respectively. This fit has been validated by calculating the energy per atom of a tube with a radius of 3 Å and comparing the DFT energy with the one predicted by the fit, the difference between the two was about 10 meV and the point is represented in red in Fig. B.4.

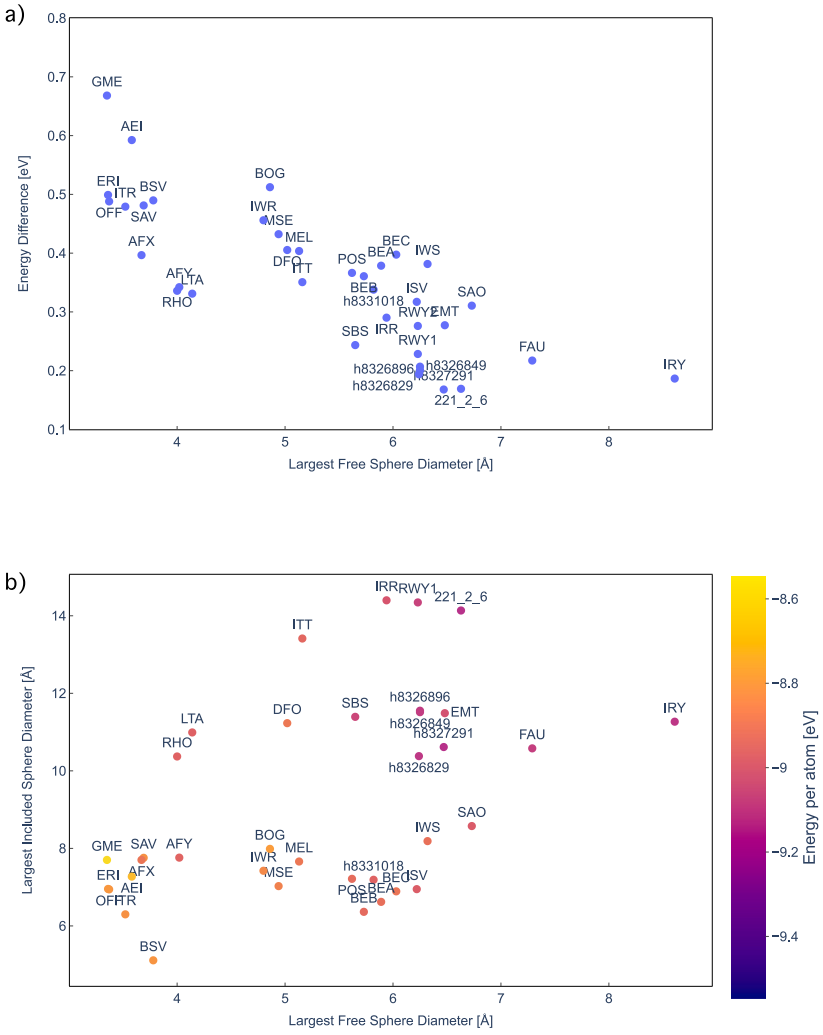

Fig. A.1. Geometry of the templates: (a) Difference in the energy per atom between each schwarzite model and diamond as a function of the largest free sphere diameter. (b) Largest included sphere diameter as a function of the largest free sphere diameter for each template; the energy per atom is depicted with the colormap.

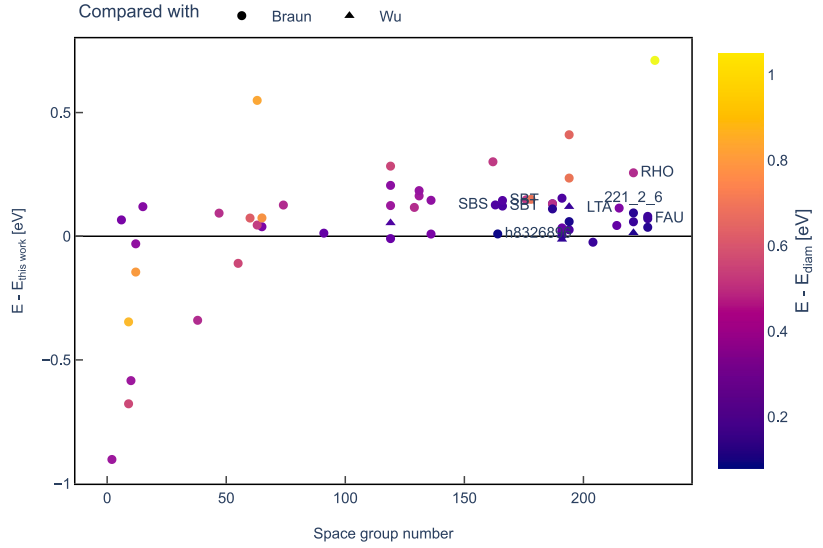

Fig. A.2. Comparison with the literature: For each template the difference in energy per atom between the models from the literature and from this work is plotted as a function of the space group number. The comparison with the models from Braun et al. [24] is plotted with a circle. The comparison with the models from Wu et al. [25] is plotted in with a triangle. The color code represents the difference in energy per atom between the structure from literature and diamond. The energies are computed with the GAP potential [46]. For the structures which are more stable than their own reference (CNT/C_{60}) the names are reported.

Table A.1
Number of atoms, total energy in eV, Energy per atom in eV, Energy difference with diamond, radius of the largest CNT (where meaningful), largest free sphere diameter, largest included sphere diameter and space group of each schwarzites models. The template space group is reported as well.

Name	Number of atoms	Total energy [eV]	Energy per atom [eV]	Energy difference diamond	Radius CNT [Å]	Df [Å]	Di [Å]	Space group	Template space group
SBT	180	−1,633.50	−9.075	0.215	2.72	5.65	11.11	166	166
FAU	168	−1,524.26	−9.073	0.217	2.74	7.29	10.58	227	227
SBS	396	−3,582.70	−9.047	0.243	2.67	5.65	11.39	163	194
221_2_6	240	−2,189.18	−9.122	0.168	3.00	6.63	14.14	221	221
IRY	408	−3,714.49	−9.104	0.186	4.06	8.61	11.27	194	194
RWY1	240	−2,174.96	−9.062	0.228	2.87	6.23	14.34	221	229
RWY2	180	−1,622.63	−9.015	0.275	2.87	6.23	14.34	204	217
EMT	420	−3,785.63	−9.013	0.277	3.40	6.48	11.49	194	194
IRR	252	−2,268.25	−9.001	0.289	5.78	5.94	14.4	191	191
SAO	120	−1,077.61	−8.980	0.310	2.84	6.73	8.58	119	119
ISV	272	−2,440.82	−8.974	0.316	2.84	6.22	6.95	131	131
LTA	96	−860.13	−8.960	0.330	/	4.14	10.99	215	221
RHO	168	−1,504.40	−8.955	0.335	/	4	10.37	221	229
AFY	96	−859.07	−8.949	0.341	2.67	4.02	7.76	162	162
ITT	228	−2,038.34	−8.940	0.350	5.72	5.16	13.41	191	191
BEB	128	−1,143.04	−8.930	0.360	2.54	5.73	6.36	15	15
POS	272	−2,427.42	−8.924	0.366	2.98	5.62	7.21	136	136
BEA	256	−2,281.50	−8.912	0.378	2.69	5.89	6.62	91	91
IWS	264	−2,352.02	−8.909	0.381	2.93	6.32	8.19	119	139
AFX	180	−1,600.94	−8.894	0.396	/	3.67	7.7	194	194
BEC	120	−1,067.19	−8.893	0.397	2.98	6.03	6.89	131	131
MEL	176	−1,564.13	−8.887	0.403	2.23	5.13	7.66	119	119
DFO	552	−4,904.74	−8.885	0.405	3.31	5.02	11.23	6	191
MSE	408	−3,614.25	−8.858	0.432	2.97	4.94	7.03	136	136
IWR	104	−918.81	−8.835	0.455	2.66	4.8	7.42	65	65
ITR	168	−1,480.35	−8.812	0.478	2.21	3.52	6.3	63	63
OFF	72	−633.80	−8.803	0.487	2.97	3.37	6.94	187	187
BSV	240	−2,112.22	−8.801	0.489	/	3.78	5.11	230	230
ERI	144	−1,266.00	−8.792	0.498	/	3.36	6.95	176	194
BOG	148	−1,299.22	−8.779	0.511	3.05	4.86	7.99	74	74
SAV	288	−2537.1551	−8.809	0.481	/	3.69	7.76	129	129
UWY	204	−1,779.86	−8.725	0.565	2.76	4.9	8.72	47	47
AEI	132	−1,148.18	−8.698	0.592	/	3.58	7.27	63	63
GME	144	−1,241.65	−8.623	0.667	3.27	3.35	7.7	194	194
h8326896	168	−1,527.08	−9.090	0.200	2.90	6.25	11.55	164	187
h8327291	150	−1,368.42	−9.123	0.167	4.52	6.47	10.61	187	187
h8326829	282	−2,565.32	−9.097	0.193	4.59	6.24	10.38	187	187
h8326849	144	−1,308.08	−9.084	0.206	3.25	6.25	11.51	191	187
h8331018	216	−1,933.81	−8.953	0.337	/	5.82	7.19	214	214
Other structures									
diamond	2	−18.58	−9.290	0.000					
C60	60	−536.30	−8.938	0.352	3.56				
cnt33	12	−106.22	−8.852	0.438	2.07				
cnt44	16	−145.97	−9.123	0.167	2.77				
cnt55	20	−183.12	−9.156	0.134	3.42				
cnt66	24	−220.96	−9.207	0.083	4.11				
cnt77	28	−258.63	−9.237	0.053	4.77				
cnt88	32	−296.06	−9.252	0.038	5.46				

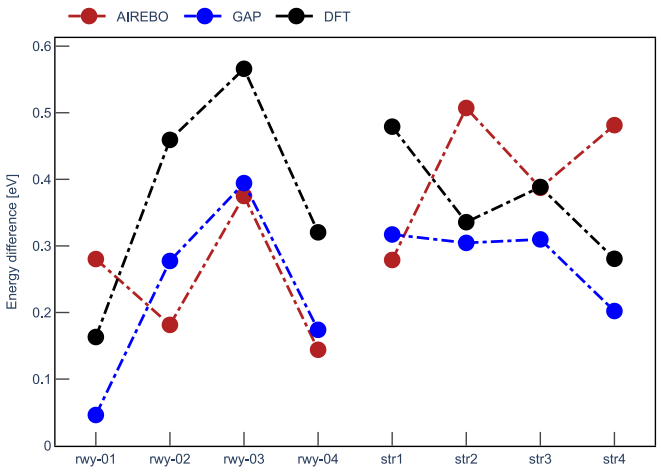

Fig. A.3. Difference in the energy per atom between a schwarzite model and diamond. Four models starting from two different zeolites are shown. Results for AIREBO are in red, for GAP in blue and for DFT in black. (For interpretation of the references to color in this figure legend, the reader is referred to the web version of this article.)

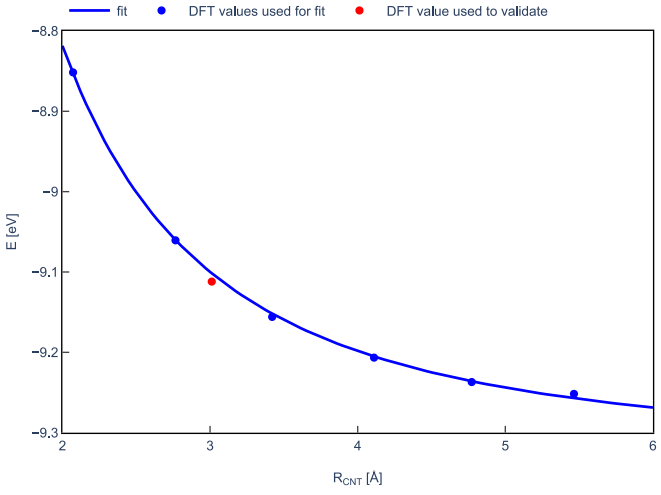

Fig. B.4. Energy fitting for carbon nanotubes. The blue dots are the six directly calculated tubes: (3,3), (4,4), (5,5), (6,6), (7,7) and (8,8). The line is the fit. The resulting fitting parameters to fill Eq. (4) are $a = -9.325$ eV and $b = 2.026$ eV $\cdot$ Å^2. The red dot is the energy per atom of the CNT used for validation. (For interpretation of the references to color in this figure legend, the reader is referred to the web version of this article.)

References

[1] H. Kroto, J. Heath, S. O'Brien, R.F. Curl, R.E. Smalley, C_{60}: Buckminsterfullerene, Nature 318 (1985) 162–163, http://dx.doi.org/10.1038/318162a0.

[2] S. Iijima, Helical microtubules of graphitic carbon, Nature 354 (1991) 56–58, http://dx.doi.org/10.1038/354056a0.

[3] S. Iijima, T. Ichihashi, Single-shell carbon nanotubes of 1-nm diameter, Nature 363 (1993) 603–605, http://dx.doi.org/10.1038/363603a0.

[4] K.S. Novoselov, A.K. Geim, S.V. Morozov, D. Jiang, Y. Zhang, et al., Electric field effect in atomically thin carbon films, Science 306 (2004) 666–669, http://dx.doi.org/10.1126/science.1102896.

[5] V. Meunier, A.G. Souza Filho, E.B. Barros, M.S. Dresselhaus, Physical properties of low-dimensional sp^2-based carbon nanostructures, Rev. Modern Phys. 88 (2016) http://dx.doi.org/10.1103/RevModPhys.88.025005, 025005–1(50).

[6] Z. Zhang, J. Chen, B. Li, Negative Gaussian curvature induces significant suppression of thermal conduction in carbon crystals, Nanoscale 9 (2017) 14208–14214, http://dx.doi.org/10.1039/c7nr04944g.

[7] L. Mackay, H. Terrones, Diamond from graphite, Nature 352 (1991) 762, http://dx.doi.org/10.1038/352762a0.

[8] D. Vanderbilt, J. Tersoff, Negative-curvature fullerene analog of C60, Phys. Rev. Lett. 68 (1992) 511–513, http://dx.doi.org/10.1103/physrevlett.68.511.

[9] T. Lenosky, X. Gonze, M. Teter, V. Elser, Energetics of negatively curved graphitic carbon, Nature 355 (1992) 333–335, http://dx.doi.org/10.1038/355333a0.

[10] M.Z. Huang, W.Y. Ching, T. Lenosky, Electronic properties of negative-curvature periodic graphitic carbon surfaces, Phys. Rev. B 47 (1993) 1593–1606, URL https://link.aps.org/doi/10.1103/PhysRevB.47.1593.

[11] H. Terrones, M. Terasaki, Curved nanostructured materials, New J. Phys. 5 (2003) 126, http://dx.doi.org/10.1088/1367-2630/5/1/126.

[12] A. Lherbier, H. Terrones, J.C. Charlier, Three-dimensional massless Dirac fermions in carbon schwarzites, Phys. Rev. B 90 (2014) 6, URL https://link.aps.org/doi/10.1103/PhysRevB.90.125434.

[13] N. Park, M. Yoon, S. Berber, J. Ihm, E. Osawa, et al., Magnetism in all-carbon nanostructures with negative Gaussian curvature, Phys. Rev. Lett. 91 (2003) 237204, URL https://link.aps.org/doi/10.1103/PhysRevLett.91.237204.

[14] S. Herkal, M.M. Rahman, S. Nagarajaiah, V.V.J. Harikrishnan, P. Ajayan, 3D printed metamaterials for damping enhancement and vibration isolation: Schwarzites, Mech. Syst. Signal Process. 185 (2023) 109819, URL https://www.sciencedirect.com/science/article/pii/S0888327022008871.

[15] H. Gong, J. Liu, K. Xu, J. Wu, Y. Li, Surface-topology-controlled mechanical characteristics of triply periodic carbon schwarzite foams, Soft Matter 16 (2020) 4324–4338, URL http://dx.doi.org/10.1039/D0SM00136H.

[16] D. Odkhuu, D.H. Jung, H. Lee, S.S. Han, S.-H. Choi, et al., Negatively curved carbon as the anode for lithium ion batteries, Carbon 66 (2014) 39–47, http://dx.doi.org/10.1016/j.carbon.2013.08.033.

[17] D.D. Borges, D.S. Galvao, Schwarzites for natural gas storage: A grand-canonical Monte Carlo study, MRS Adv. 3 (2018) 115–120, http://dx.doi.org/10.1557/adv.2018.190.

[18] P.O. Krasnov, G.S. Shkaberina, S.P. Polyutov, Molecular hydrogen sorption capacity of P216-Schwarzite: PM6-D3, MP2 and QTAIM approaches, Comput. Mater. Sci. 209 (2022) 111410, URL https://www.sciencedirect.com/science/article/pii/S092702562200180X.

[19] Z. Zhang, S. Hu, T. Nakayama, J. Chen, B. Li, Reducing lattice thermal conductivity in Schwarzites via engineering the hybridized phonon modes, Carbon 139 (2018) 289–298, URL https://www.sciencedirect.com/science/article/pii/S0008622318306237.

[20] H. Nishihara, T. Kyotani, Templated nanocarbons for energy storage, Adv. Mater. 24 (2012) 4473–4498, http://dx.doi.org/10.1002/adma.201201715.

[21] H. Nishihara, T. Kyotani, Novel Carbon Adsorbents, Elsevier, Amsterdam, 2012, pp. 295–322,

[22] H. Nishihara, T. Kyotani, Zeolite-templated carbons – three-dimensional microporous graphene frameworks, Chem. Commun. 54 (2018) 5648–5673, http://dx.doi.org/10.1039/C8CC01932K.

[23] H. Nishihara, Q.-H. Yang, P.-X. Hou, M. Unno, S. Yamauchi, et al., A possible buckybowl-like structure of zeolite templated carbon, Carbon 47 (2009) 1220–1230, http://dx.doi.org/10.1016/j.carbon.2008.12.040.

[24] E. Braun, Y. Lee, S.M. Moosavi, S. Barthel, R. Mercado, et al., Generating carbon Schwarzites via zeolite-templating, Proc. Natl. Acad. Sci. 115 (2018) E8116–E8124, http://dx.doi.org/10.1073/pnas.1805062115.

[25] J. Wu, K. Zhang, H. Yoo, Y. Lee, In silico generation of a topologically diverse zeolite-templated carbon library, Cryst. Growth and Des. 22 (2022) 123–130, http://dx.doi.org/10.1021/acs.cgd.1c00620.

[26] A. Buekenhoudt, A. Kovalevsky, J. Luyten, F. Snijkers, Basic aspects in inorganic membrane preparation, in: E. Drioli, L. Giorno (Eds.), Comprehensive Membrane Science and Engineering, Elsevier, Oxford, ISBN: 978-0-08-093250-7, 2010, pp. 217–252, http://dx.doi.org/10.1016/b978-0-08-093250-7.00011-6.

[27] Yujie Liu, Elisabet Huertas Osta, Artem S. Poryvaev, Matvey V. Fedin, Alessandro Longo, Alexei Nefedov, Nikolay Kosinov, Direct conversion of methane to zeolite-templated carbons, light hydrocarbons, and hydrogen, Carbon 201 (2023) 535–541, URL https://www.sciencedirect.com/science/article/pii/S0008622322007746.

[28] N. Wang, Z.K. Tang, G.D. Li, J.S. Chen, Single-walled 4 Å carbonnanotube arrays, Nature 408 (2000) 50–51, http://dx.doi.org/10.1038/35040702.

[29] E.E. Taylor, K. Garman, N.P. Stadie, Atomistic structures of zeolite-templated carbon, Chem. Mater. 32 (2020) 2742–2752, http://dx.doi.org/10.1021/acs.chemmater.0c00535.

[30] J.M. Farrell, V. Grande, D. Schmidt, F. Würthner, A highly warped heptagon-containing sp2 carbon scaffold via vinylnaphthyl π-extension, Angew. Chem. Int. Ed. 58 (46) (2019) 16504–16507, URL https://onlinelibrary.wiley.com/doi/abs/10.1002/anie.201909975.

[31] Y. Segawa, H. Ito, K. Itam, Structurally uniform and atomically precise carbon nanostructures, Nat. Rev. Mater. 1 (2016) 15002, http://dx.doi.org/10.1038/natrevmats.2015.2.

[32] M.W. Wang, Z. Li, Y. Liu, W. Jiang, Z. Wang, Precise synthesis of schwarzite carbon: hypothesis or reality? Org. Chem. Front. 10 (2023) 2808–2812, http://dx.doi.org/10.1039/D3QO00202K.

[33] R.M. Tromer, L.C. Felix, C.F. Woellner, D.S. Galvao, On the structural stability and optical properties of germanium-based schwarzites: A density functional theory investigation, Phys. Chem. Chem. Phys. 22 (2020) 16286–16293, http://dx.doi.org/10.1039/D0CP02143A.

[34] Ch. Baerlocher, L.B. McCusker, Database of zeolite structures, 2017, http://www.iza-structure.org/databases/. (Accessed March 2022).

[35] C.J. Pickard, Ephemeral data derived potentials for random structure search, Phys. Rev. B 106 (2022) 014102, URL https://link.aps.org/doi/10.1103/PhysRevB.106.014102.
[36] C.J. Pickard, R.J. Needs, Ab initio random structure searching, J. Phys.: Condens. Matter 23 (2011) 053201, http://dx.doi.org/10.1088/0953-8984/23/5/053201.
[37] A.R. Organov, C.J. Pickard, Q. Zhu, R.J. Needs, Structure prediction drives materials discovery, Nat. Rev. 4 (2019) 331–348, http://dx.doi.org/10.1038/s41578-019-0101-8.
[38] V.S. Urusov, T.N. Nadezhina, Frequency distribution and selection of space groups in inorganic crystal chemistry, J. Struct. Chem. 50 (2009) S22–S37, http://dx.doi.org/10.1007/s10947-009-0186-9.
[39] MODL UCLouvain, RandomCarbon Python code, 2023, https://github.com/modl-uclouvain/randomcarbon. (Accessed May 2023).
[40] R.D. Shannon, Revised effective ionic radii and systematic studies of interatomic distances in halides and chalcogenides, Acta Cryst. A32 (1976) 751–767, http://dx.doi.org/10.1107/S0567739476001551.
[41] S. Katoch, S.S. Chauhan, V. Kumar, A review on genetic algorithm: past, present, and future, Multimedia Tools Appl. 80 (2021) 8091—8126, http://dx.doi.org/10.1007/s11042-020-10139-6.
[42] B.C. Revard, W.W. Tipton, A. Yesypenko, R.G. Henning, Grand-canonical evolutionary algorithm for the prediction of two-dimensional materials, Phys. Rev. B 93 (2016) 054117, http://dx.doi.org/10.1103/PhysRevB.93.054117.
[43] W.W. Tipton, R.G. Henning, A grand canonical genetic algorithm for the prediction of multi-component phase diagrams and testing of empirical potentials, J. Phys.: Condens. Matter 25 (2013) 495401, http://dx.doi.org/10.1088/0953-8984/25/49/495401.
[44] L.B. Vilhelmsen, K.S. Walton, D.S. Sholl, Structure and mobility of metal clusters in MOFs: Au, Pd, and AuPd clusters in MOF-74, J. Am. Chem. Soc. 134 (2012) 12807–12816, http://dx.doi.org/10.1021/ja305004a.
[45] S.J. Stuart, A.B. Tutein, J.A. Harrison, A reactive potential for hydrocarbons with intermolecular interactions, J. Chem. Phys. 112 (14) (2000) 6472–6486, http://dx.doi.org/10.1063/1.481208.
[46] P. Rowe, V.L. Deringer, P. Gasparotto, G. Csányi, A. Michaelides, An accurate and transferable machine learning potential for carbon, J. Chem. Phys. 153 (2020) 034702, http://dx.doi.org/10.1063/5.0005084.
[47] G. Kresse, J. Hafner, Ab initio molecular dynamics for liquid metals, Phys. Rev. B 47 (1993) URL https://link.aps.org/doi/10.1103/PhysRevB.47.558.
[48] G. Kresse, J. Hafner, Ab initio molecular-dynamics simulation of the liquid-metal–amorphous-semiconductor transition in germanium, Phys. Rev. B 49 (1994) 14251–14269, URL https://link.aps.org/doi/10.1103/PhysRevB.49.14251.
[49] G. Kresse, J. Furthmüller, Efficiency of ab-initio total energy calculations for metals and semiconductors using a plane-wave basis set, Comput. Mater. Sci. 6 (1996) 15–50, http://dx.doi.org/10.1016/0927-0256(96)00008-0.
[50] G. Kresse, J. Furthmüller, Efficient iterative schemes for ab initio total-energy calculations using a plane-wave basis set, Phys. Rev. B 54 (1996) 11169–11186, URL https://link.aps.org/doi/10.1103/PhysRevB.54.11169.
[51] S. Grimme, J. Antony, S. Ehrlich, H. Krieg, A consistent and accurate ab initio parametrization of density functional dispersion correction (DFT-D) for the 94 elements H-Pu, J. Chem. Phys. 132 (2010) http://dx.doi.org/10.1063/1.3382344.
[52] K. Mathew, J.H. Montoya, A. Faghaninia, S. Dwarakanath, M. Aykol, et al., Atomate: A high-level interface to generate, execute, and analyze computational materials science workflows, Comput. Mater. Sci. 139 (2017) 140–152, http://dx.doi.org/10.1016/j.commatsci.2017.07.030.
[53] Atomate2 github repository, 2023, https://github.com/materialsproject/atomate2. (Accessed 03 April 2023).
[54] A. Jain, S.P. Ong, W. Chen, B. Medasani, X. Qu, et al., FireWorks: a dynamic workflow system designed for high-throughput applications, Concurr. Comput.: Pract. Exper. 27 (2015) 5037–5059, http://dx.doi.org/10.1002/cpe.3505.
[55] L.C. Qin, X. Zhao, K. Hirahara, Y. Miyamoto, Y. Ando, et al., The smallest carbon nanotube, Nature 408 (2000) 50, http://dx.doi.org/10.1038/35040699.
[56] Z.K. Tang, L. Zhang, N. Wang, X.X. Zhang, G.H. Wen, et al., Superconductivity in 4 Angstrom single-walled carbon nanotubes, Science 292 (2001) 2462–2465, http://dx.doi.org/10.1126/science.1060470.
[57] T.F. Willems, C.H. Rycroft, M. Kazi, J.C. Meza, M. Haranczyk, Algorithms and tools for high-throughput geometry-based analysis of crystalline porous materials, Microporous Mesoporous Mater. 149 (2012) 134–141, http://dx.doi.org/10.1016/j.micromeso.2011.08.020.
[58] X. Li, A. Wang, K.R. Lee, Comparison of empirical potentials for calculating structural properties of amorphous carbon films by molecular dynamics simulation, Comput. Mater. Sci. 151 (2018) 246–254, http://dx.doi.org/10.1016/j.commatsci.2018.04.062.
[59] E. Marazzi, A. Ghojavand, J. Pirard, G. Petretto, J.-C. Charlier, G.-M. Rignanese, Modeling symmetric and defect-free carbon schwarzites into various zeolite templates, Mater. Cloud Arch. 2023.138 (2023) http://dx.doi.org/10.24435/materialscloud:r0-ef.
[60] Modelling symmetric and defect-free carbon schwarzites into various zeolite templates - website, 2023, https://schwarzites.modl-uclouvain.org. (Accessed 25 July 2023).
[61] G. Fraux, R.K. Cersonsky, M. Ceriotti, Chemiscope: interactive structure-property explorer for materials and molecules, J. Open Source Softw. 5 (2020) 2117, http://dx.doi.org/10.21105/joss.02117.